Electronic Supplementary Information (ESI)

Significant hydrogen generation via photo-mechanical coupling in flexible methylammonium lead iodide nanowires

Yucheng Zhang,[a] Jiawei Huang,[a] Mengya Zhu,[b] Zhouyang Zhang,[b] Kaiqi Nie,[c] Zhiguo Wang,[a] Xiaxia Liao,[a] Longlong Shu,[a] Tingfang Tian,*[a] Zhao Wang,*[d] Yang Lu,[e] and Linfeng Fei *[a]

[a] School of Physics and Materials Science, Nanchang University, Nanchang 330031, China

[b] Department of Mechanical Engineering, City University of Hong Kong, Kowloon, Hong Kong SAR, China

[c] Institute of High Energy Physics, Chinese Academy of Sciences, Beijing 100049, China

[d] Hubei Key Laboratory of Micro-& Nanoelectronic Materials and Devices, School of Microelectronics, Hubei University, Wuhan 430062, China

[e] Department of Mechanical Engineering, The University of Hong Kong, Hong Kong SAR, China

E-mail: feilinfeng@gmail.com (L. F. Fei); wangzhao@hubu.edu.cn (Z. Wang); tftian@ncu.edu.cn (T. F. Tian)

Contents of Supplementary Information:

Methods

Synthesis of $MAPbI_3$ NWs

461.1 mg PbI_2 powder was added into 1 mL N,N-dimethylformamide (DMF) before the system was heated to 70 °C on a hot plate for 1 h, while in another reactor, 159 mg MAI (C_4H_6IN) was added into 20 mL isopropyl alcohol (IPA) and vigorously stirred at room temperature for 30 min under an argon atmosphere. After that, the PbI_2 solution was gradually added to the MAI solution. The mixture was vigorously stirred under an atmosphere of argon for 30 minutes; and finally, $MAPbI_3$ NWs were obtained by centrifuging the mixture.

Synthesis of $MAPbI_3$ NPs

MAI and PbI_2 of 1:1 molar ratio were dissolved in DMF in a vial and stirred for 2 hours before the formation of a yellow solution. $MAPbI_3$ NPs were synthesized by adding the precursor solution drop by drop to toluene. The solvent was then removed at a centrifugal rate of 8000 rpm for 5 minutes. The product was then collected after drying at 70 °C in a vacuum oven.

Synthesis of $MAPbI_3$ SCs

2.0 M PbI_2 and 2.0 M MAI were dissolved in a mixed solvent of DMSO–DMF (7:3 by volume; DMSO: dimethyl sulfoxide) in a vial. The precursor solution was then filtered with a polytetrafluoroethylene (PTFE) filter before heating on an oil bath at 70 °C for a period of time in order to produce $MAPbI_3$ SCs. For example, small SCs (average size about 1.5 mm) can be harvested by maintaining 5 ml precursor solution at this temperature for 5 hours.

General characterizations

XRD patterns were obtained on a Rigaku D/Max diffractometer with a Cu K_α radiation. SEM images were obtained on a Thermos Scientific Scios2 dual beam electron microscope operated at 20 kV. TEM images and EDS elemental mappings were obtained on a 300 kV double aberration-corrected Titan Themis Z electron microscope. UPS measurements were conducted in the 4B9B beamline at Beijing Synchrotron Radiation Facility with He I source (21.2 eV). The spectra were collected using a Scienta R4000 spectrometer with an energy resolution better than 0.1 eV. For the work function measurements, all samples were biased at −5 eV to acquire the low cutoff of secondary electron. The photon energy was calibrated by the Au $4f_{7/2}$ peak with a binding energy of 84 eV. UV–Vis DRS spectra were recorded on a Hitachi UH-4150 UV–Vis spectrophotometer with spectral-grade $BaSO_4$ as a reference.

In situ PFM test

In situ PFM test was performed on a NT-MDT scanning probe microscopy (SPM, NT-MDT Ntegra upright) with a heating stage (SU045NTF, NT-MDT, Russia) which was equipped with a Pt resistor to achieve its temperature stability at 0.05 °C. By moving the probe tip of PFM to the middle region of the scanned NW, the displacement-voltage butterfly curve and the phase curve were obtained upon applying a voltage in a certain range at each temperature.

In situ bending test

A batch of NWs was dispersed in isopropanol by stirring and ultrasonication to get a dilute suspension, which was then drop-casted onto a copper grid. Using the Model 450PM Manual Probe Station platform, an appropriate NW was picked with the help of a light microscopy, which was then experienced a force on one tip by a fine tungsten needle.

Finite element simulations

Finite element simulations were performed using a COMSOL software. The length of $MAPbI_3$ NW was set to 30 μm, and the diameter was set to 300 nm. The elastic modulus and Poisson's ratio of the $MAPbI_3$ NW were set to 20 GPa and 0.4, respectively. The NW was simply supported at both ends, and the axial displacement constraint was set at the bottom to ensure that the NW can bend freely. The bending of the NW was realized by applying bending moments at both ends. The bending moment was set to 10^{-12} N m in order to approach the level of strain gradient in our experiments.

Hydrogen evolution test

First, a saturated HI solution was prepared as follows. An H-shaped cell was employed in this preparation to separate the anode and cathode compartment with a Nafion 117 membrane placed between them. 10 mL of 57 wt% HI solution was added in each compartment. 2.97 g PbI_2 was dissolved in the HI at the cathode compartment and stirred at 60 °C before slowly adding 1.025 g MAI. Carbon fiber papers with an active area of 4 cm^2 were utilized as both the working and counter electrodes. After Ar gas purging into two compartments for 15 min, −800 mA of current was applied on the working electrode for 2 h (**Figure S16**). Thereafter, the saturated hydrogen iodide solution was obtained in the cathode compartment.

Subsequently, the hydrogen production rates were determined from a homemade top-lighting reactor (30 ml; with water cooling). A 300 W Xe-lamp (PLS-SXE 300/300UV, Beijing Perfect Light, China) with a 420 nm cut-off filter was used as a visible light source, and mechanical stimulation was introduced to the reactor by a magnetic stirrer at 300 rpm. Typically, 50 mg $MAPbI_3$ NWs was dispersed into 5 ml saturated HI solution for a single hydrogen evolution test. The evolved H_2 was

quantitatively analyzed by a gas chromatograph (Shimadzu GC-2014) with Ar as the carrier gas.

Calculation of the catalytic efficiency

By utilizing the concentration of HI solution and the computed free energy associated with splitting the solution, we can determine the potential energy value, denoted as E_{HI}, which equals to 0.33 eV. Utilizing this potential energy value, we can evaluate the solar conversion efficiency of our photomechanocatalytic reaction by utilizing the following equation.[1, 2]

$$\text{Solar HI splitting efficiency (\%)} = \frac{\left[\text{Evolved } H_2\,(\text{mol}) \times 6.02 \times 10^{23} \times 2 \times 0.330\,(\text{eV}) \times 1.6 \times 10^{-19}\right]}{[\text{Psol (W cm}^{-2}) \times \text{Area (cm}^2) \times \text{time (s)}]} \times 100\%$$

For instance, in the case of the $MAPbI_3$ NWs deposited, 75.65 μmol of H_2 could be generated after 2 h of light irradiance at 100 mW cm^{-2}. Because our light irradiation area was 0.25 cm^2, the solar HI splitting efficiency could be calculated as 2.67%.

Supplementary Figures

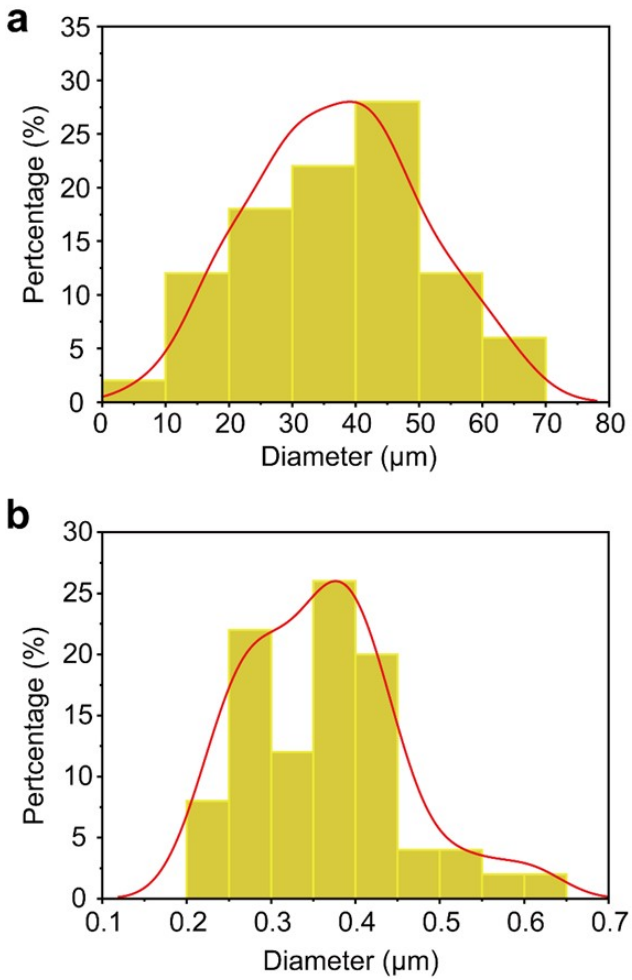

Fig. S1 Statistics of lengths and diameters for $MAPbI_3$ NWs. (a) Length statistics of $MAPbI_3$ NWs. (b) Diameter statistics of $MAPbI_3$ NWs.

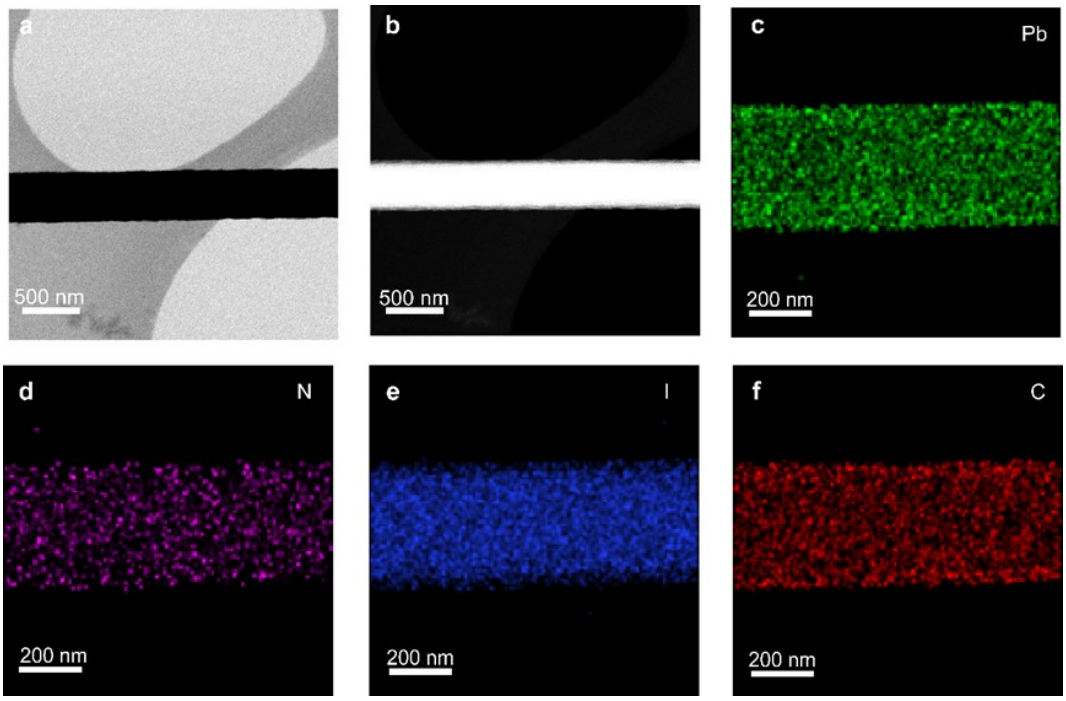

Fig. S2 Morphological characterization and elemental distributions of $MAPbI_3$ NWs. (a) TEM image of a NW. (b-f) STEM (i.e., scanning transmission electron microscopy) image and the EDS elemental mappings for Pb, N, I, and C.

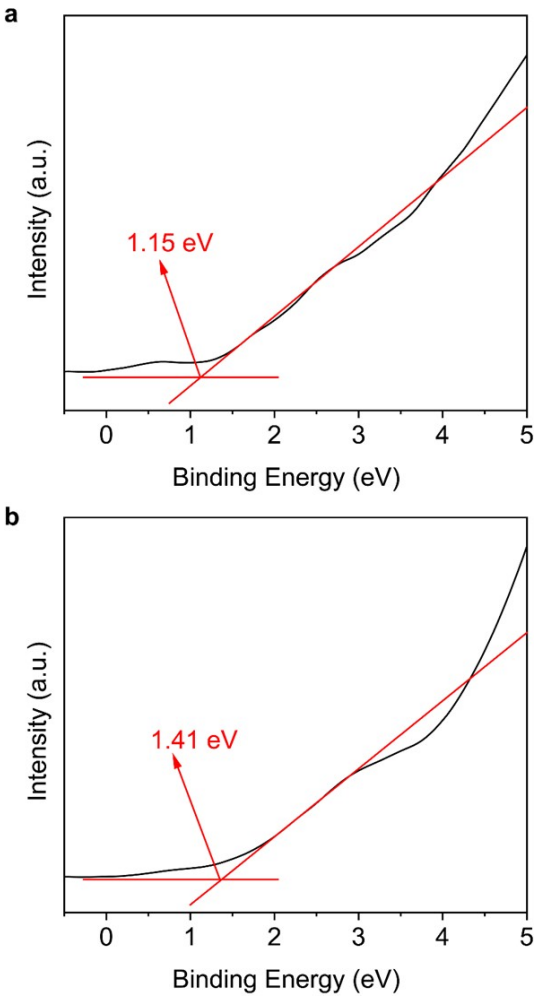

Fig. S3 UPS characterizations for (a) $MAPbI_3$ SC and (b) $MAPbI_3$ NPs.

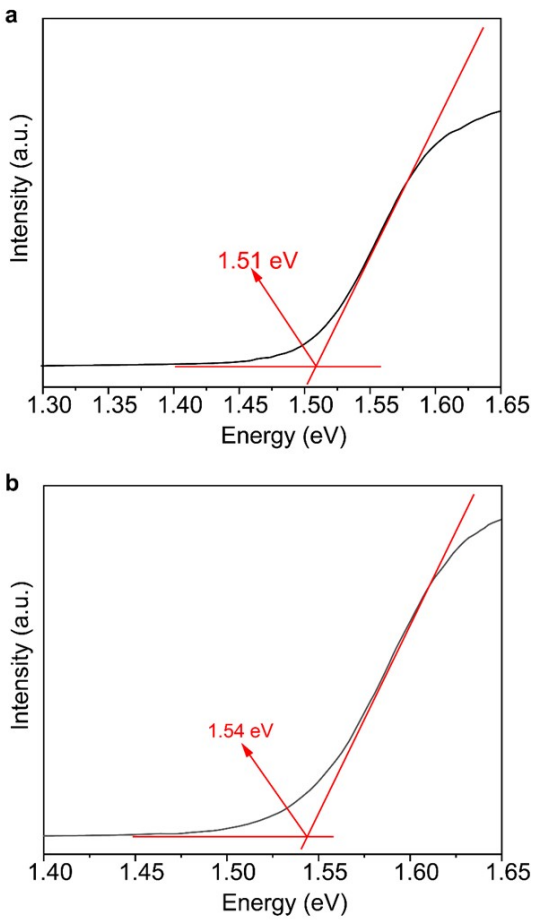

Fig. S4 Tauc plots for (a) $MAPbI_3$ SC and (b) $MAPbI_3$ NPs.

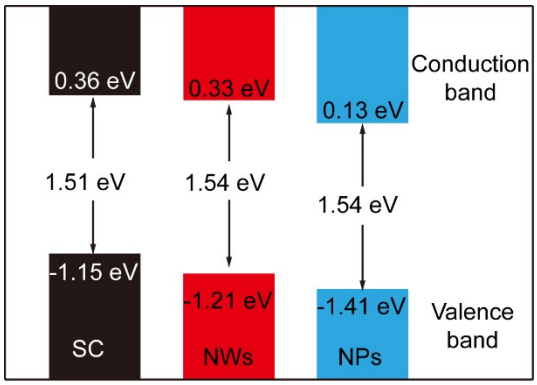

Fig. S5 Comparison of the structures of optical bandgaps (versus Fermi level) for $MAPbI_3$ SC, NWs and NPs.

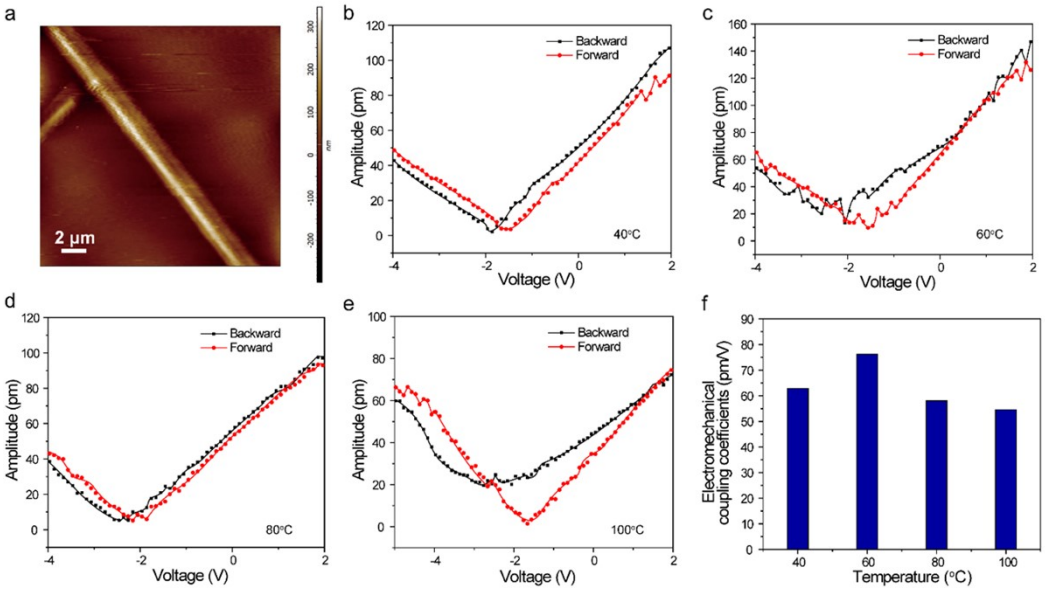

Fig. S6 In situ PFM response of NWs at a temperature range from RT to 100 °C. (a) The corresponding PFM morphology image for a $MAPbI_3$ NW. (b) PFM amplitude response for a $MAPbI_3$ NW at 40 °C. (c) PFM amplitude response for a $MAPbI_3$ NW at 60 °C. (d) PFM amplitude response for a $MAPbI_3$ NW at 80 °C. (e) PFM amplitude response for a $MAPbI_3$ NW at 100 °C. (f) Electromechanical coupling coefficients for the above NW from RT to 100°C.

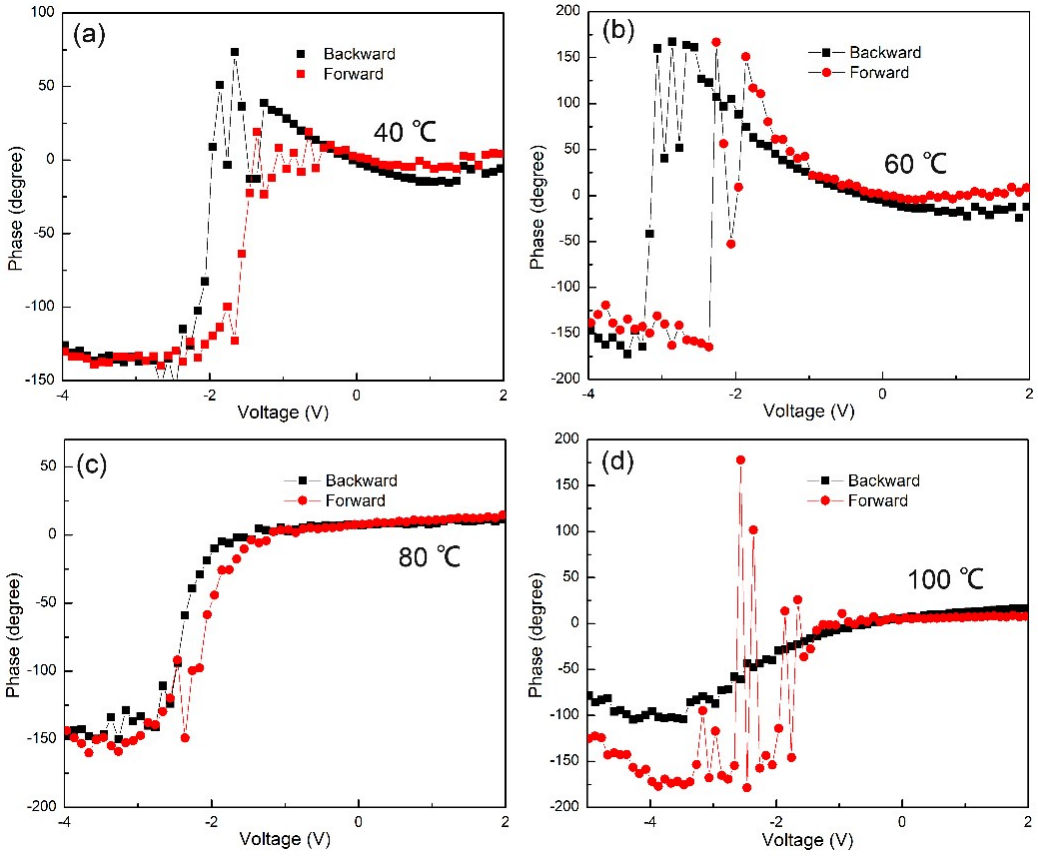

Fig. S7 The phase-voltage curves of a $MAPbI_3$ NW tested by PFM at (a) 40 °C, (b) 60 °C, (c) 80 °C, and (d) 100 °C.

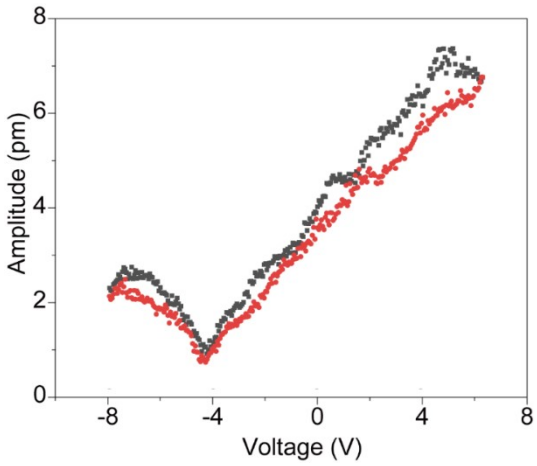

Fig. S8 PFM amplitude response of a commercial $LiNbO_3$ sample.

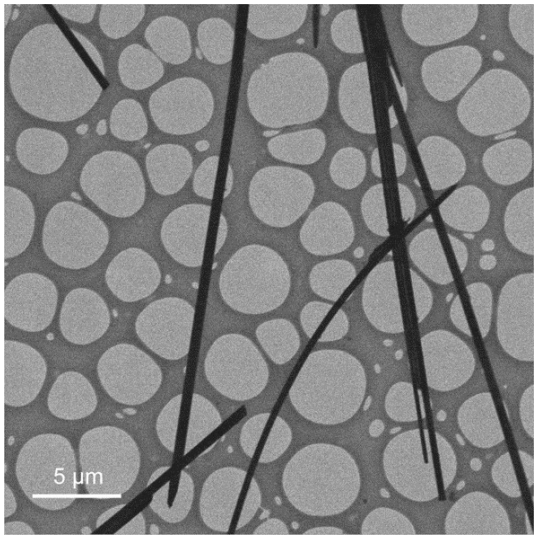

Fig. S9 Bright-field TEM image for $MAPbI_3$ NWs, in which the bending NW can be observed.

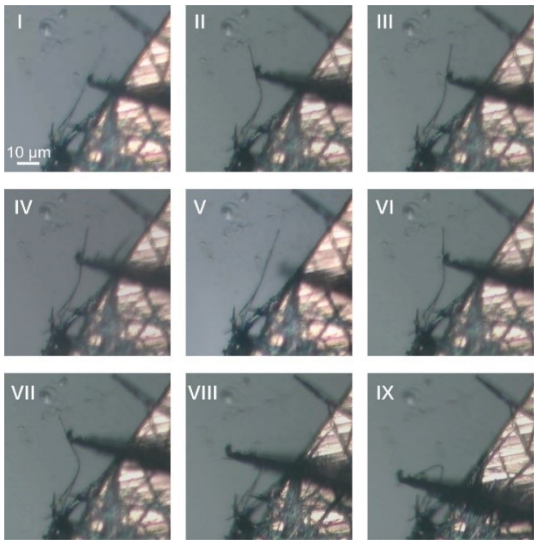

Fig. S10 Optical image series showing a $MAPbI_3$ NW experienced multiple bending-recovery processes before it was broken.

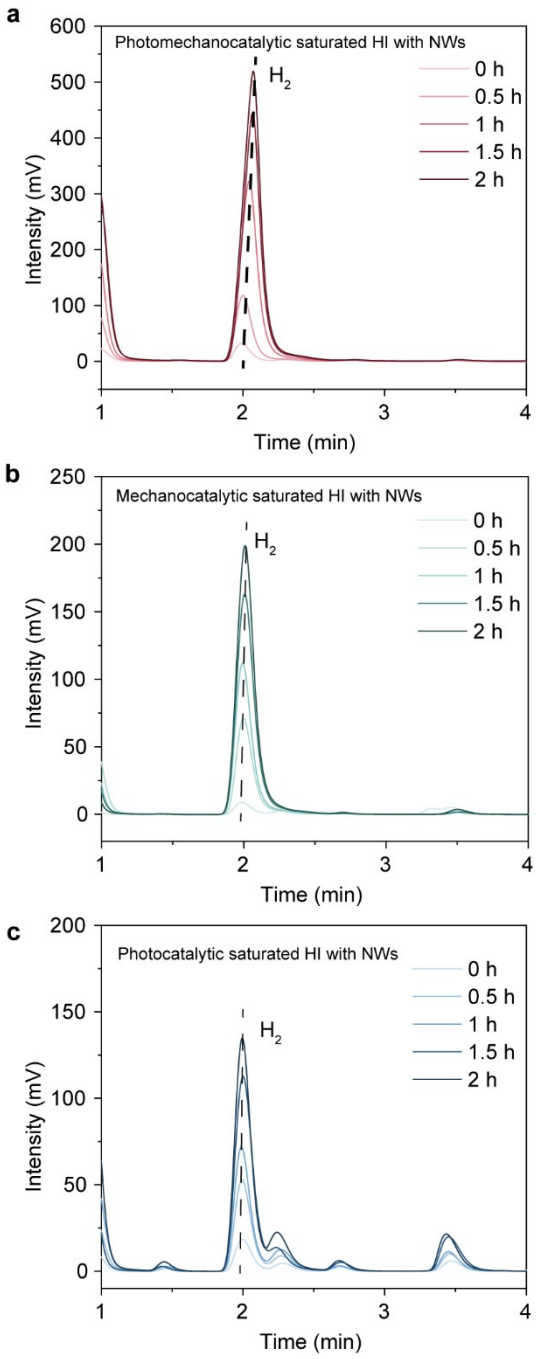

Fig. S11 GC data for hydrogen gas production from the decomposition of saturated HI using $MAPbI_3$ NWs under photomechanocatalytic, mechanocatalytic, and photocatalytic conditions. (a) $MAPbI_3$ NWs decompose saturated HI under a photomechanocatalytic condition. (b) $MAPbI_3$ NWs decompose saturated HI under a mechanocatalytic condition. (c) $MAPbI_3$ NWs decompose saturated HI under a photocatalytic condition.

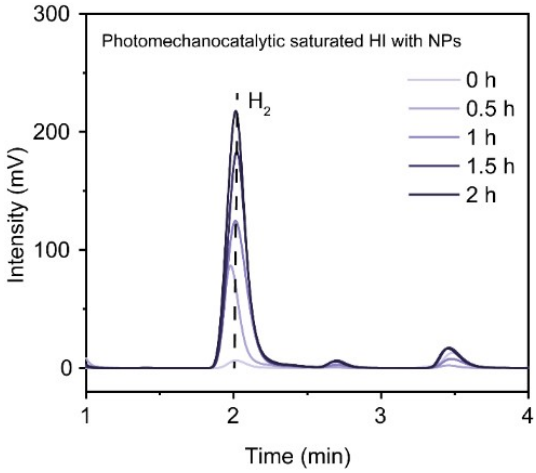

Fig. S12 $MAPbI_3$ NPs decompose saturated HI under a photomechanocatalytic condition.

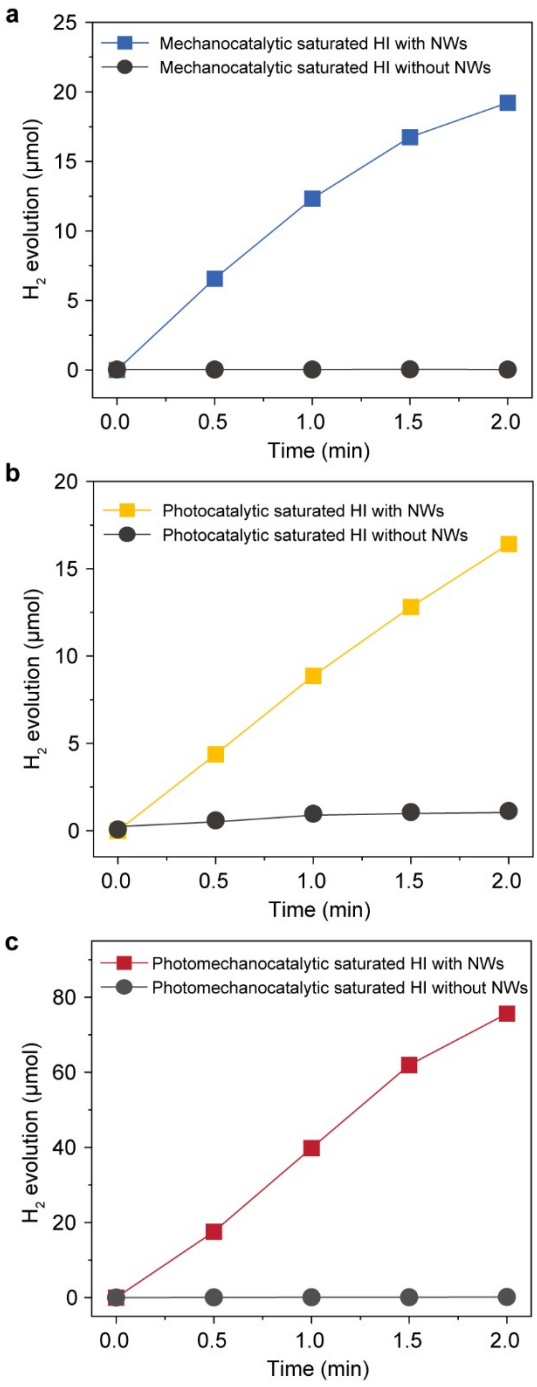

Fig. S13 HI splitting by the NWs in a saturated HI solution at various conditions. (a) Mechanocatalytic HI splitting reaction of the saturated solution in the presence and absence of $MAPbI_3$ NWs. (b) Photocatalytic HI splitting reaction of the saturated solution in the presence and absence of $MAPbI_3$ NWs. (c) Photomechanocatalytic HI splitting reaction of the saturated solution in the presence and absence of $MAPbI_3$ NWs.

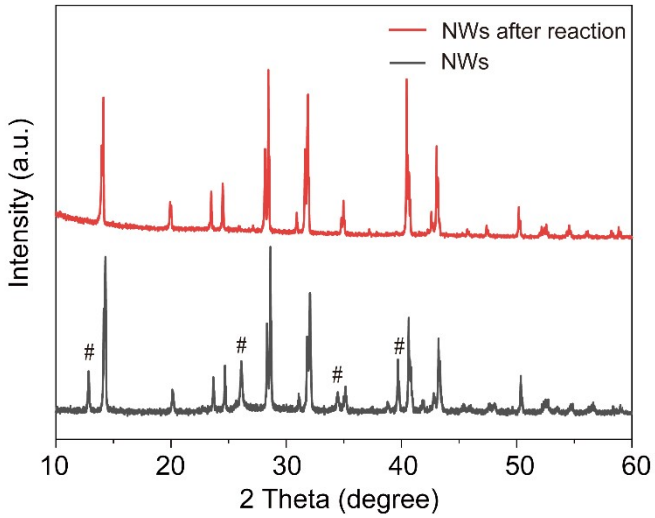

Fig. S14 XRD patterns for $MAPbI_3$ NWs before and after the catalytic reaction.

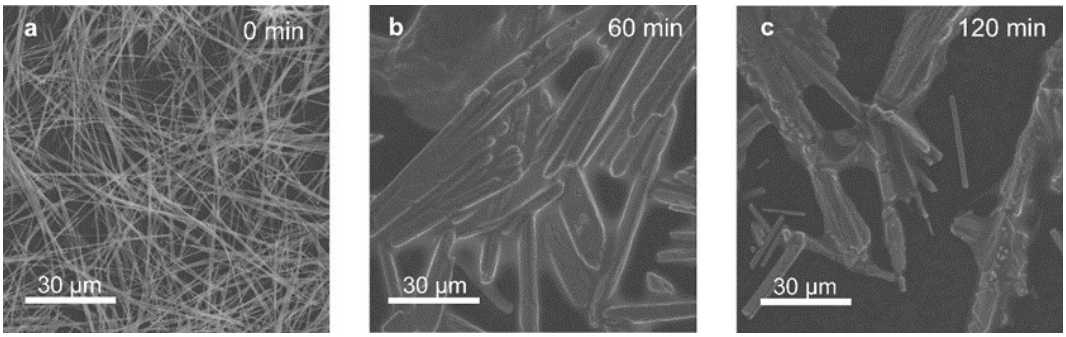

Fig. S15 Structural characterization of NWs before and after the catalytic reaction. (a) SEM image of $MAPbI_3$ NWs at 0 min. (b) SEM image of $MAPbI_3$ NWs after 60 min of catalytic reaction. (c) SEM of $MAPbI_3$ NWs at 120 min of catalytic reaction.

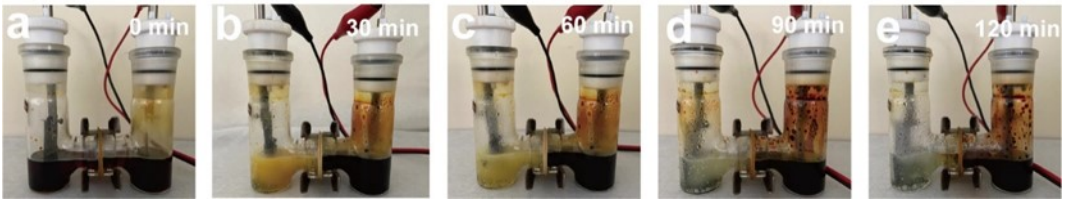

Fig. S16 Photos for the electrical reduction process of saturated HI.

Table. S1 A summary of previously reported typical catalysts and their performance in the hydrogen evolution reaction from HI decomposition.

Catalyst	Light source	Precious metal	Catalytic Mechanism	Activity [H_2 μmol g^{-1} h^{-1}]	Year [Reference]
$MAPbI_3$ NWs	300 W Xe lamp (λ ≥ 420 nm)	---	Photo-mechano-	756.5	This work
$MAPbI_3$/Pt	Solar simulator (λ > 475nm)	Pt	Photo-	57.0	2016[1]
$MAPbI_3$/Pt/TiO_2	300 W Xe lamp (200 mW cm^{-2}, λ ≥ 420 nm)	Pt	Photo-	5293	2018[3]
$MAPbBr_{3-x}I_x$/Pt	300 W Xe lamp (λ ≥ 420 nm)	Pt	Photo-	2604	2018[4]
$MAPbI_3$/rGO	300 W Xe lamp (120 mW cm^{-2}, λ ≥ 420 nm)	---	Photo-	939	2018[5]
$MABi_2I_9$/Pt	300 W Xe lamp (λ ≥ 400 nm)	Pt	Photo-	169	2019[6]
$MAPbI_3$/black phosphorus	Xe lamp (300 mW cm^{-2}, λ ≥ 420 nm)	---	Photo-	3742	2019[7]
Pt/Ta_2O_5/$MAPbBr_3$/PEDOT:PSS	300 W Xe lamp (150 mW cm^{-2}, λ ≥ 420 nm)	Pt	Photo-	619	2019[8]
$MAPbI_3$	500 W Xe lamp (100 mW cm^{-2})	---	Photo-	68.4	2019[9]
$MAPbI_3$	500 W Xe lamp (100 mW cm^{-2})	---	Piezo-	44.2	2019[9]
$MAPbI_3$	500 W Xe lamp (100 mW cm^{-2})	---	Piezophoto-	460.7	2019[9]
$MAPbI_3$/Ni_3C	300 W Xe lamp (λ > 420nm)	---	Photo	2362	2019[10]
$MAPb(Br_{0.1}I_{0.9})_3$/Pt	300 W Xe lamp (λ ≥ 420 nm)	Pt	Photo-	3348	2019[11]
$MAPbI_3$/CoP	150 W Xe lamp (λ > 420nm)	---	Photo-	785.9	2020[12]
$Cs_3Bi_{2x}Sb_{2-2x}I_9$/Pt	Solar simulator	Pt	Photo-	926	2020[13]
$MAPbI_3$/Pt/C	10 W LED lamp (380 ≤λ≤780 nm)	---	Photo-	685	2020[14]
$Cs_3Bi_2I_9$	450 W Xe lamp (150 mW cm^{-2})	---	Photo-	225	2022[15]

1T-2H $MoSe_2$ modified $MAPbI_3$	300 W Xe lamp (λ > 420nm)	---	Photo-	552.9	2022[16]

References

1. S. Park, W. J. Chang, C. W. Lee, S. Park, H.-Y. Ahn and K. T. Nam, Photocatalytic hydrogen generation from hydriodic acid using methylammonium lead iodide in dynamic equilibrium with aqueous solution, *Nat. Energy*, 2016, **2**, 16185.
2. W. Guan, Y. Li, Q. Zhong, H. Liu, J. Chen, H. Hu, K. Lv, J. Gong, Y. Xu, Z. Kang, M. Cao and Q. Zhang, Fabricating $MAPbI_3/MoS_2$ composites for improved photocatalytic performance, *Nano Lett.*, 2021, **21**, 597-604.
3. X. Wang, H. Wang, H. Zhang, W. Yu, X. Wang, Y. Zhao, X. Zong and C. Li, Dynamic interaction between methylammonium lead Iodide and TiO_2 nanocrystals leads to enhanced photocatalytic H_2 evolution from HI splitting, *ACS Energy Lett.*, 2018, **3**, 1159-1164.
4. Y. Wu, P. Wang, Z. Guan, J. Liu, Z. Wang, Z. Zheng, S. Jin, Y. Dai, M.-H. Whangbo and B. Huang, Enhancing the photocatalytic hydrogen evolution activity of mixed-halide perovskite $CH_3NH_3PbBr_{3-x}I_x$ achieved by bandgap funneling of charge carriers, *ACS Catal.*, 2018, **8**, 10349-10357.
5. Y. Wu, P. Wang, X. Zhu, Q. Zhang, Z. Wang, Y. Liu, G. Zou, Y. Dai, M.-H. Whangbo and B. Huang, Composite of $CH_3NH_3PbI_3$ with reduced graphene oxide as a highly efficient and stable visible-light photocatalyst for hydrogen evolution in aqueous HI solution, *Adv. Mater.*, 2018, **30**, 1704342.
6. Y. Guo, G. Liu, Z. Li, Y. Lou, J. Chen and Y. Zhao, Stable lead-free $(CH_3NH_3)_3Bi_2I_9$ perovskite for photocatalytic hydrogen generation, *ACS Sustainable Chem. Eng.*, 2019, **7**, 15080-15085.
7. R. Li, X. Li, J. Wu, X. Lv, Y.-Z. Zheng, Z. Zhao, X. Ding, X. Tao and J.-F. Chen, Few-layer black phosphorus-on-$MAPbI_3$ for superb visible-light photocatalytic hydrogen evolution from HI splitting, *Appl. Catal., B*, 2019, **259**, 118075.
8. H. Wang, X. Wang, R. Chen, H. Zhang, X. Wang, J. Wang, J. Zhang, L. Mu, K. Wu, F. Fan, X. Zong and C. Li, Promoting photocatalytic H_2 evolution on organic–inorganic hybrid perovskite nanocrystals by simultaneous dual-charge transportation modulation, *ACS Energy Lett.*, 2019, **4**, 40-47.
9. M. Wang, Y. Zuo, J. Wang, Y. Wang, X. Shen, B. Qiu, L. Cai, F. Zhou, S. P. Lau and Y. Chai, Remarkably enhanced hydrogen generation of organolead halide perovskites via piezocatalysis and photocatalysis, *Adv. Energy Mater.*, 2019, **9**, 1901801.
10. Z. Zhao, J. Wu, Y.-Z. Zheng, N. Li, X. Li and X. Tao, Ni_3C-decorated $MAPbI_3$ as visible-light photocatalyst for H_2 evolution from HI splitting, *ACS Catal.*, 2019, **9**, 8144-8152.

11. Z. Zhao, J. Wu, Y.-Z. Zheng, N. Li, X. Li, Z. Ye, S. Lu, X. Tao and C. Chen, Stable hybrid perovskite $MAPb(I_{1-x}Br_x)_3$ for photocatalytic hydrogen evolution, *Appl. Catal., B*, 2019, **253**, 41-48.
12. C. Cai, Y. Teng, J.-H. Wu, J.-Y. Li, H.-Y. Chen, J.-H. Chen and D.-B. Kuang, In situ photosynthesis of an $MAPbI_3$/CoP hybrid heterojunction for efficient photocatalytic hydrogen evolution, *Adv. Funct. Mater.*, 2020, **30**, 2001478.
13. G. Chen, P. Wang, Y. Wu, Q. Zhang, Q. Wu, Z. Wang, Z. Zheng, Y. Liu, Y. Dai and B. Huang, Lead-free halide perovskite $Cs_3Bi_{2x}Sb_{2-2x}I_9$ ($x \approx 0.3$) possessing the photocatalytic activity for hydrogen evolution comparable to that of $(CH_3NH_3)PbI_3$, *Adv. Mater.*, 2020, **32**, 2001344.
14. F. Wang, X. Liu, Z. Zhang and S. Min, A noble-metal-free MoS_2 nanosheet-coupled $MAPbI_3$ photocatalyst for efficient and stable visible-light-driven hydrogen evolution, *Chem. Commun.*, 2020, **56**, 3281-3284.
15. S. P. Chaudhary, S. Bhattacharjee, V. Hazra, S. Shyamal, N. Pradhan and S. Bhattacharyya, $Cs_3Bi_2I_9$ nanodiscs with phase and $Bi_{(III)}$ state stability under reductive potential or illumination for H_2 generation from diluted aqueous HI, *Nanoscale*, 2022, **14**, 4281-4291.
16. T. Zhang, Y. Cai, Y. Lou and J. Chen, 1T-2H $MoSe_2$ modified $MAPbI_3$ for effective photocatalytic hydrogen evolution, *J. Alloys Compd.*, 2022, **893**, 162329.